Anwendungen

Oliver Fritsch*, David Tromba, and Boris Lohmann

Cascaded energy based trajectory tracking control of a quadrotor

Kaskadierte energiebasierte Trajektorienfolgeregelung eines Quadrocopters

Abstract: This paper presents a cascaded nonlinear state feedback control law for a quadrotor, which achieves asymptotic tracking of a predefined position and heading reference trajectory. The inner-loop attitude controller and the outer-loop position controller reflect the cascade structure of the quadrotor dynamics and are designed independently using an energy shaping approach. The closed loop tracking error dynamics form a nonautonomous nonlinear cascade for whose zero equilibrium we prove almost global asymptotic stability. Experimental results show the performance of the control concept.

Keywords: Nonlinear cascaded control, energy shaping, quadrotor UAV.

Zusammenfassung: In diesem Beitrag wird eine nichtlineare Kaskadenregelung für einen Quadrocopter vorgestellt, die asymptotische Sollwertfolge für eine vorgegebene Positions- und Headingtrajektorie erzielt. Der innere Lageregler und der äußere Positionsregler spiegeln die Kaskadenstruktur der Regelstrecke wider und werden unabhängig voneinander energiebasiert entworfen. Die resultierende Folgefehlerdynamik bildet eine nichtautonome nichtlineare Kaskade, für deren Gleichgewichtspunkt in Null fast globale asymptotische Stabilität gezeigt wird. Flugversuchsdaten illustrieren die Leistungsfähigkeit der Regelung.

Schlüsselwörter: Nichtlineare Kaskadenregelung, energiebasierte Regelung, Quadrocopter.

DOI 10.1515/auto-2013-1063
Received September 4, 2013; accepted March 11, 2014

***Corresponding Author: Oliver Fritsch,** Technische Universität München, e-mail: oliver.fritsch@tum.de
David Tromba, Boris Lohmann: Technische Universität München

1 Introduction

In recent years, the technological progress concerning lightweight structures, efficient aerodynamics as well as new propulsion and energy storage systems has significantly accelerated the development of autonomous operating unmanned aerial vehicles and in particular vertical take-off and landing aircrafts (VTOLs). In combination with improving methods of flight guidance and control the scope of application is constantly growing and comprises fields like cartography, meteorological measurements, emergency management, aerial imaging for movies and television broadcasts, photogrammetry, surveillance and many more. These tasks are executed at different autonomy levels of flight control ranging from simple remote controlled flight to fully autonomous mission accomplishment [9].

In this paper we develop a flight control system enabling a quadrotor (see Figure 1) to autonomously track a predefined position and heading trajectory. To solve this control task many control schemes such as feedback linearization [6, 8], sliding mode control [16], geometric control [17], backstepping [4, 19], forwarding [3], adaptive control [1, 24] as well as cascaded control [2, 11, 23] have been proposed for VTOLs in the literature. In view of the cascade structure of the quadrotor dynamics, the latter obviously represents a very natural approach to the control problem and will be used in this work. However, the expression *cascaded control* only refers to the hierarchical structure of the overall controller, which divides into independent subsystem controllers. In fact, arbitrary control approaches can be used for the design of the nested control loops. The resulting segmentation of the problem into subproblems and the excess of flexibility regarding the control approaches reduces the complexity and facilitates the tuning of the subsystem controllers. This is what makes cascaded control appealing. In return, the stability properties of the overall system do not arise directly from the design of the subsystem controllers but have to be es-

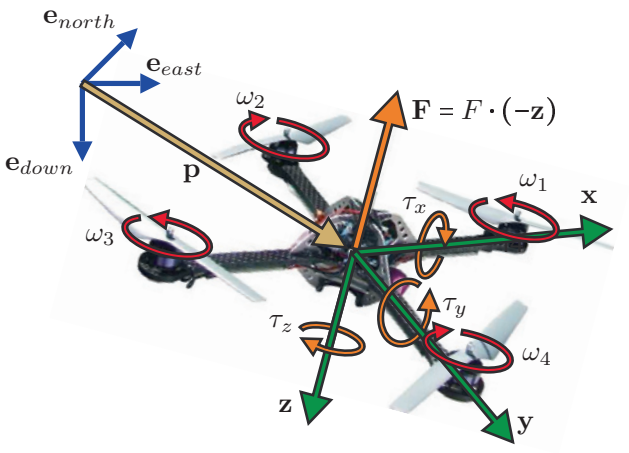

Figure 1: Quadrotor with body-fixed frame $B = \{\mathbf{x}, \mathbf{y}, \mathbf{z}\}$, inertial frame $I = \{\mathbf{e}_{north}, \mathbf{e}_{east}, \mathbf{e}_{down}\}$ and control inputs $F, \tau_x, \tau_y, \tau_z$.

tablished a posteriori by showing compliance with a set of assumptions.

Regarding the quadrotor, the cascaded control comprises a position and an attitude control loop. This reflects the quadrotor's cascade structure. Like most rotary-wing aerial vehicles, quadrotors are underactuated mechanical systems with six degrees of freedom and four control inputs, in detail the magnitude of the thrust force and three control torques. The translational dynamics are driven by the thrust force, with only the magnitude being directly controllable and the direction being governed by the underlying attitude dynamics. The latter in turn are accessible via the control torques. Accordingly, one can split up the controller design into the design of an outer position control loop and an inner attitude control loop. The position controller regards the thrust force as a virtual control input and forwards its direction as one part of the attitude reference input to the inner-loop. Complemented by a desired heading trajectory, the attitude reference input is then tracked by the inner attitude controller. The resulting tracking error dynamics form a nonautonomous nonlinear cascade, consisting of the independent attitude error subsystem which couples into the position error subsystem via an interconnection term. Due to this coupling, the stability properties of the uncoupled subsystems do not necessarily propagate to the cascade. A widely spread reasoning for the use of cascaded controllers is the assumption of a time-scale separation between a fast inner control loop and rather slow outer control loop. This would imply that the effect of the interconnection is weak and stability bounds could be estimated using for instance singular perturbation techniques [15]. Especially in modern technological applications with increasing performance requirements this assumption is questionable. Therefore, we rigorously prove the stability properties of our closed loop adapting mainly the results of [27] and [26] on nonlinear cascade systems to our problem. The final stability check amounts to showing compliance of the controlled system with a set of assumptions.

In contrast to previously presented cascaded controllers for the problem [2, 11, 23], we do not use local attitude parameterizations like Euler angles but we consider the attitude on its natural domain $SO(3)$. As a consequence the attitude control law which is taken from the previous work [5] is singularity free, whereas the control laws of the stated references unavoidably contain singularities mostly hidden in the input transformations that are performed. A further difference is the use of energy shaping and damping injection techniques for the design of the subsystem controllers.

By a suitable shaping of the potential energy and the injection of a sophisticated damping, this approach enables us to design an outer-loop position controller, which satisfies constraints on the maximal and minimal thrust force. In particular, the controller can be prevented from commanding a zero thrust force. This way, a common obstacle in quadrotor control is circumvented, because only a nonzero thrust force guarantees that the direction of the thrust is always well defined. This in turn is a requirement for a valid attitude reference. Finally, in contrast to the other references we are able to show that the zero tracking error is almost globally asymptotically stable (AGAS), which means that its region of attraction comprises the whole state space except for a nowhere dense set of measure zero [14].

The remainder of the paper is organized as follows. In Section 2 we introduce the notation used and give some preliminary definitions. The quadrotor dynamics and the problem statement are presented in Section 3, before we derive the tracking error dynamics in Section 4. In Section 5 a stability result for a class of cascade systems including our problem is established. Sections 6 and 7 are devoted to the controller design for the position subsystem and to the specification of an appropriate control law for the magnitude of the thrust. The controller for the attitude subsystem is adopted from [5] and hence only briefly addressed in Section 8. Experimental results are shown in Section 9 and in Section 10 we summarize our results.

2 Nomenclature and definitions

We indicate scalars as italic letters, whereas vectors and matrices are indicated by upright bold letters. Any vec-

tor $\mathbf{a} \in \mathbb{R}^3$ that designates a physical quantity (like e. g. a position) without referring to a certain coordinate frame is denoted as an *abstract* vector. General geometric relations can (and will) be discussed using abstract vectors. To assign numerical values to an abstract vector a suitable coordinate frame has to be chosen. All coordinate frames used are right-handed Cartesian coordinate systems and identified by uppercase italic letters. The representation of an abstract vector $\mathbf{a} \in \mathbb{R}^3$ with respect to a certain frame $E = \{\mathbf{e}_1, \mathbf{e}_2, \mathbf{e}_3\}$ with orthonormal basis vectors $\mathbf{e}_1, \mathbf{e}_2, \mathbf{e}_3$ is denoted by $\mathbf{a}_E$. For some vectors, which are exclusively represented in one coordinate frame, the basis designation will be dropped and thus the distinction to their abstract representations is given up. Additionally, we define the basis independent unit vectors $\mathbf{e}_x = \begin{bmatrix}1 & 0 & 0\end{bmatrix}^T$, $\mathbf{e}_y = \begin{bmatrix}0 & 1 & 0\end{bmatrix}^T$ and $\mathbf{e}_z = \begin{bmatrix}0 & 0 & 1\end{bmatrix}^T$. The transformation from a frame E to another frame E' is given by a rotation matrix $\mathbf{R}_{E'E} \in SO(3)$, where $SO(3) = \{\mathbf{R} \in \mathbb{R}^{3\times3} : \mathbf{R}^T\mathbf{R} = \mathbf{I}_3, \det(\mathbf{R}) = 1\}$ is the special orthogonal group and $\mathbf{I}_i$, $i \in \mathbb{N}$ denotes the $i \times i$ identity matrix. Sometimes it is convenient to consider a rotation matrix as a vector. For any $\mathbf{R} = \begin{bmatrix}\mathbf{r}_1 & \mathbf{r}_2 & \mathbf{r}_3\end{bmatrix} \in SO(3)$ we define $\vec{\mathbf{R}} = \begin{bmatrix}\mathbf{r}_1^T & \mathbf{r}_2^T & \mathbf{r}_3^T\end{bmatrix}^T$. The angular velocity of a frame E' with respect to a frame E given in a frame E'' is denoted by $\boldsymbol{\omega}_{E''}^{EE'} \in \mathbb{R}^3$. We also define the skew symmetric operator $\langle\!\langle \cdot \rangle\!\rangle : \mathbb{R}^3 \to \mathfrak{so}(3)$, where $\mathfrak{so}(3) = \{\mathbf{K} \in \mathbb{R}^{3\times3} : \mathbf{K}^T = -\mathbf{K}\}$, such that for any vector $\mathbf{a} = \begin{bmatrix}a_x & a_y & a_z\end{bmatrix}^T$ it holds that

$$\langle\!\langle \mathbf{a} \rangle\!\rangle = \begin{bmatrix} 0 & -a_z & a_y \\ a_z & 0 & -a_x \\ -a_y & a_x & 0 \end{bmatrix}. \tag{1}$$

Accordingly, $\langle\!\langle \mathbf{a} \rangle\!\rangle \mathbf{b} = \mathbf{a} \times \mathbf{b}$ reflects the cross product for $\mathbf{a}, \mathbf{b} \in \mathbb{R}^3$. The inverse operator is $\rangle\!\rangle \cdot \langle\!\langle : \mathfrak{so}(3) \to \mathbb{R}^3$. For vectors $\mathbf{a} = \begin{bmatrix}\mathbf{a}_1^T & \mathbf{a}_2^T & \mathbf{a}_3^T\end{bmatrix}^T \in \mathbb{R}^9$, where $\mathbf{a}_1, \mathbf{a}_2, \mathbf{a}_3 \in \mathbb{R}^3$ we define $\langle\!\langle \mathbf{a} \rangle\!\rangle = \begin{bmatrix}\langle\!\langle \mathbf{a}_1 \rangle\!\rangle^T & \langle\!\langle \mathbf{a}_2 \rangle\!\rangle^T & \langle\!\langle \mathbf{a}_3 \rangle\!\rangle^T\end{bmatrix}^T$. The unit sphere of dimension $i \in \mathbb{N}$ is denoted by $\mathcal{S}^i = \{\mathbf{a} \in \mathbb{R}^{i+1} : \mathbf{a}^T\mathbf{a} = 1\}$. Our notation for the boundary of a set $\mathcal{A}$ is $\partial\mathcal{A}$. For any $\mathbf{a} \in \mathbb{R}^n$ the Euclidean norm is indicated as $\|\mathbf{a}\|$. We will also make use of two one-sided saturation functions, shown in Figure 2. Let $\underline{a}, \bar{a}$ and Δ_a be positive constants and let $\bar{\alpha} = {}^{\Delta_a}\!/_{\bar{a}}$ and $\underline{\alpha} = {}^{\Delta_a}\!/_{\underline{a}}$. Then, by $\bar{\sigma}_{\Delta_a}^{\bar{a}} : \mathbb{R} \to]-\infty, \bar{a}]$ we denote the C^2 saturation function

$$\bar{\sigma}_{\Delta_a}^{\bar{a}}(a) = \begin{cases} a & \text{if} \quad a \le \bar{a} - \Delta_a \\ P_4(a) & \text{if} \quad \bar{a} - \Delta_a < a \le \bar{a} + \Delta_a \\ \bar{a} & \text{if} \quad a > \bar{a} + \Delta_a, \end{cases} \tag{2}$$

where $P_4(a)$ is the fourth order polynomial

$$P_4(a) = \frac{\bar{a}}{\bar{\alpha}^3}\left(\frac{3}{48}\left(\frac{a}{\bar{a}}\right)^4 - \frac{3}{12}\left(\frac{a}{\bar{a}}\right)^3 - \frac{3\bar{\alpha}^2 - 3}{8}\left(\frac{a}{\bar{a}}\right)^2 - \frac{2\bar{\alpha}^3 + 3\bar{\alpha}^2 - 1}{4}\left(\frac{a}{\bar{a}}\right) + \frac{3\bar{\alpha}^4 - 8\bar{\alpha}^3 + 6\bar{\alpha}^2 - 1}{16}\right). \tag{3}$$

By $\underline{\sigma}_{\Delta_a}^{a} : \mathbb{R} \to [\underline{a}, \infty[$ we denote the C^1 saturation function

$$\underline{\sigma}_{\Delta_a}^{a}(a) = \begin{cases} \underline{a} & \text{if } a \le \underline{a} - \Delta_a \\ P_2(a) & \text{if } \underline{a} - \Delta_a < a \le \underline{a} + \Delta_a \\ a & \text{if } a > \underline{a} + \Delta_a, \end{cases} \tag{4}$$

where $P_2(a)$ is the second order polynomial

$$P_2(a) = \frac{\underline{a}}{\underline{\alpha}}\left(\frac{1}{4}\left(\frac{a}{\underline{a}}\right)^2 + \frac{\underline{\alpha} - 1}{2}\left(\frac{a}{\underline{a}}\right) + \frac{\underline{\alpha}^2 + 2\underline{\alpha} + 1}{4}\right). \tag{5}$$

We will frequently encounter the case that a (scalar, vector or matrix) quantity a can be given as a function $f(\cdot)$ of coordinates $\mathbf{b}$, i. e. $a = f(\mathbf{b})$, and also as a function $\tilde{f}(\cdot)$ of coordinates $\mathbf{c}$, i. e. $a = \tilde{f}(\mathbf{c})$. With a slight abuse of notation we will write $a(\mathbf{b})$ to refer to $f(\mathbf{b})$ and $a(\mathbf{c})$ to refer to $\tilde{f}(\mathbf{c})$.

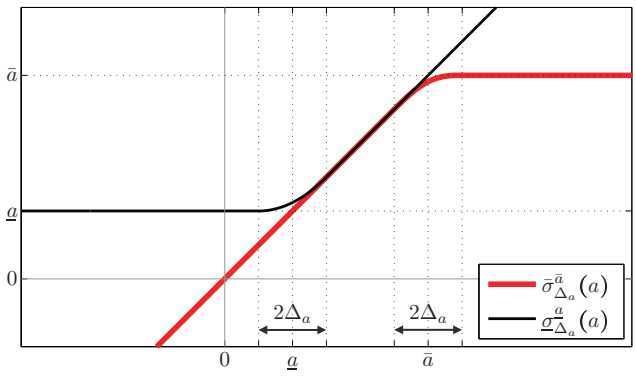

Figure 2: Saturation functions.

3 Problem statement

Regarding the quadrotor as a rigid body, we consider an inertial north east down frame $I = \{\mathbf{e}_{north}, \mathbf{e}_{east}, \mathbf{e}_{down}\}$ and a body-fixed frame $B = \{\mathbf{x}, \mathbf{y}, \mathbf{z}\}$ attached to the center of gravity of the quadrotor as shown in Figure 1. Then, the configuration of the quadrotor is given by the position vector $\mathbf{p} \in \mathbb{R}^3$ and the rotation matrix $\mathbf{R}_{BI} = \begin{bmatrix}\mathbf{x}_I & \mathbf{y}_I & \mathbf{z}_I\end{bmatrix}^T$. The rigid body dynamics are

$$m\ddot{\mathbf{p}}_I = -\mathbf{D}\dot{\mathbf{p}}_I + mg\mathbf{e}_z - F\mathbf{z}_I \tag{6}$$

$$\dot{\mathbf{R}}_{BI} = -\langle\!\langle \boldsymbol{\omega}_B^{IB} \rangle\!\rangle \mathbf{R}_{BI} \tag{7}$$

$$\mathbf{J}\dot{\boldsymbol{\omega}}_B^{IB} = -\langle\!\langle \boldsymbol{\omega}_B^{IB} \rangle\!\rangle \mathbf{J}\boldsymbol{\omega}_B^{IB} + \boldsymbol{\tau}, \tag{8}$$

where m is the mass of the quadrotor, the constant matrix $\mathbf{D} \geq 0$ models the aerodynamic drag, g is the gravitational acceleration and $\mathbf{J}$ is the quadrotor's moment of inertia matrix with respect to the center of gravity given in B. The magnitude F of the thrust force $\mathbf{F} = F \cdot (-\mathbf{z})$ and the torque vector $\boldsymbol{\tau} = \begin{bmatrix} \tau_x & \tau_y & \tau_z \end{bmatrix}^T$ are considered as the control variables of the system. This is based on the common assumption that there exists a known one to one relation $(F, \boldsymbol{\tau}) = \mathbf{f}(\omega_1^2, \omega_2^2, \omega_3^2, \omega_4^2)$ (see e. g. [29]) linking F and $\boldsymbol{\tau}$ to the squares of the rotor angular rates $\omega_i, i \in \{1, 2, 3, 4\}$, which are the real control variables. It is assumed that the state variables $\mathbf{p}_I$, $\dot{\mathbf{p}}_I$, $\mathbf{R}_{BI}$, and $\boldsymbol{\omega}_B^{IB}$ are either directly measurable or provided by an appropriate data fusion.

The primary control objective is to let the quadrotor track a desired position trajectory $\mathbf{p}_d$, i. e. $\mathbf{p} \to \mathbf{p}_d$ as $t \to \infty$. This obviously requires an appropriate manipulation of the thrust force $\mathbf{F} = F \cdot (-\mathbf{z})$, where only the magnitude F is directly controlled and $\mathbf{z}$ depends on the quadrotor's current attitude. This reveals the quadrotor's inherent cascade structure consisting of the position independent attitude dynamics (7), (8) controlled by $\boldsymbol{\tau}$ and the translational dynamics (6) depending on $\mathbf{z}_I$, which is the last row of $\mathbf{R}_{BI}$. We will make use of this structure by developing a cascaded controller consisting of an outer position controller considering a desired thrust force $\mathbf{F}_d = F_d \cdot (-\mathbf{z}_d)$ as a virtual control variable and an inner attitude controller responsible to track the desired z-axis direction $\mathbf{z}_d$.

It remains to specify the orientation around $\mathbf{z}_d$ to define a complete desired frame $D = \{\mathbf{x}_d, \mathbf{y}_d, \mathbf{z}_d\}$ to be tracked by the attitude controller. This degree of freedom is used to achieve the secondary control objective concerning the heading. The desired heading trajectory is specified in terms of the vector $\mathbf{h}_{d,I} = \begin{bmatrix} h_{d,Ix} & h_{d,Iy} & 0 \end{bmatrix}^T \in \mathbb{S}^2$ lying in the horizontal plane. The desired x-axis direction $\mathbf{x}_d$ is obtained by the normalized projection of $\mathbf{h}_d$ along $\mathbf{e}_{down}$ onto the plane perpendicular to $\mathbf{z}_d$, see Figure 3 (a). Noting that $\mathbf{e}_{down,I} = \mathbf{e}_z$, one may verify that

$$\mathbf{x}_{d,I} = \frac{1}{\| \langle\!\langle \langle\!\langle \mathbf{e}_z \rangle\!\rangle \mathbf{h}_{d,I} \rangle\!\rangle \mathbf{z}_{d,I} \|} \langle\!\langle \langle\!\langle \mathbf{e}_z \rangle\!\rangle \mathbf{h}_{d,I} \rangle\!\rangle \mathbf{z}_{d,I} \tag{9}$$

holds. The desired frame D is completed by $\mathbf{y}_d = \langle\!\langle \mathbf{z}_d \rangle\!\rangle \mathbf{x}_d$ and parametrized by the rotation matrix $\mathbf{R}_{ID} = \begin{bmatrix} \mathbf{x}_{d,I} & \mathbf{y}_{d,I} & \mathbf{z}_{d,I} \end{bmatrix}$. In terms of the error rotation matrix $\mathbf{R}_{BD} = \mathbf{R}_{BI}\mathbf{R}_{ID}$ the control objective of the attitude controller is $\mathbf{R}_{BD} \to \mathbf{I}_3$ as $t \to \infty$. For the heading vector $\mathbf{h}$, which is the orthogonal projection of $\mathbf{x}$ onto the horizontal plane (see Figure 3 (b)), this means $\mathbf{h} \to \mathbf{h}_d$ as $t \to \infty$.

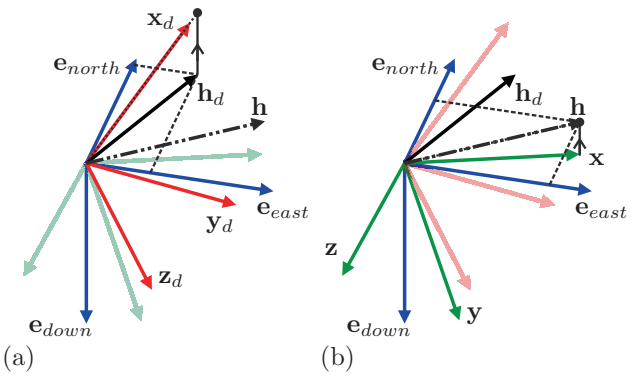

Figure 3: Both figures show the same situation. (a) Specification of $\mathbf{x}_d$ by projecting $\mathbf{h}_d$ onto the plane normal to $\mathbf{z}_d$ and normalization. (b) Construction of $\mathbf{h}$ by projecting $\mathbf{x}$ onto the horizontal plane and normalization.

4 Tracking error dynamics

The relative motion between the desired frame D and the body-fixed frame B is determined by the attitude tracking dynamics. As shown in [5], they are derived using the attitude kinematics and Euler's equation and can be written as

$$\dot{\mathbf{R}}_{BD} = -\langle\!\langle \boldsymbol{\omega}_B^{DB} \rangle\!\rangle \mathbf{R}_{BD} \tag{10}$$

$$\dot{\boldsymbol{\omega}}_B^{DB} = \dot{\boldsymbol{\omega}}_B^{IB} - \dot{\boldsymbol{\omega}}_B^{ID} = \mathbf{J}^{-1}\left(-\langle\!\langle \boldsymbol{\omega}_B^{IB} \rangle\!\rangle \mathbf{J}\boldsymbol{\omega}_B^{IB} + \boldsymbol{\tau}\right) - \dot{\boldsymbol{\omega}}_B^{ID}. \tag{11}$$

It was also shown in [5] that $\boldsymbol{\omega}_B^{DB}$ and $\dot{\boldsymbol{\omega}}_B^{ID}$ are obtained from the known quantities as

$$\boldsymbol{\omega}_B^{DB} = \Big\rangle\!\Big\rangle \langle\!\langle \boldsymbol{\omega}_B^{IB} \rangle\!\rangle - \mathbf{R}_{BI}\dot{\mathbf{R}}_{ID}\mathbf{R}_{ID}^T\mathbf{R}_{BI}^T \Big\langle\!\Big\langle \tag{12}$$

$$\begin{aligned} \dot{\boldsymbol{\omega}}_B^{ID} = \Big\rangle\!\Big\rangle & - \langle\!\langle \boldsymbol{\omega}_B^{IB} \rangle\!\rangle \mathbf{R}_{BI}\dot{\mathbf{R}}_{ID}\mathbf{R}_{ID}^T\mathbf{R}_{BI}^T \\ & + \mathbf{R}_{BI}\ddot{\mathbf{R}}_{ID}\mathbf{R}_{ID}^T\mathbf{R}_{BI}^T + \mathbf{R}_{BI}\dot{\mathbf{R}}_{ID}\dot{\mathbf{R}}_{ID}^T\mathbf{R}_{BI}^T \\ & + \mathbf{R}_{BI}\dot{\mathbf{R}}_{ID}\mathbf{R}_{ID}^T\mathbf{R}_{BI}^T\langle\!\langle \boldsymbol{\omega}_B^{IB} \rangle\!\rangle \Big\langle\!\Big\langle . \end{aligned} \tag{13}$$

We now define the rotational tracking error vector

$$\mathbf{x}_R = \begin{bmatrix} \tilde{\mathbf{R}} \\ \boldsymbol{\omega}_B^{DB} \end{bmatrix} = \begin{bmatrix} \vec{\mathbf{R}}_{BD} - \vec{\mathbf{I}}_3 \\ \boldsymbol{\omega}_B^{DB} \end{bmatrix} \in \mathcal{M} \subset \mathbb{R}^{12}, \tag{14}$$

where $\mathcal{M}$ with $\dim(\mathcal{M}) = 6$ is a smooth manifold. By applying the input transformation

$$\boldsymbol{\tau} = \langle\!\langle \boldsymbol{\omega}_B^{IB} \rangle\!\rangle \mathbf{J}\boldsymbol{\omega}_B^{IB} + \mathbf{J}\dot{\boldsymbol{\omega}}_B^{ID} + \tilde{\boldsymbol{\tau}} \tag{15}$$

one deduces from (14), (10) and (11) that the attitude tracking error dynamics can be represented as

$$\dot{\mathbf{x}}_R = \underbrace{\begin{bmatrix} \langle\!\langle \tilde{\mathbf{R}} + \vec{\mathbf{I}}_3 \rangle\!\rangle \boldsymbol{\omega}_B^{DB} \\ \mathbf{J}^{-1}\tilde{\boldsymbol{\tau}} \end{bmatrix}}_{\mathbf{f}_R(\mathbf{x}_R, \tilde{\boldsymbol{\tau}})}, \tag{16}$$

where $\tilde{\boldsymbol{\tau}}$ is the new input. In Section 8 we briefly address a partial-feedback control law $\tilde{\boldsymbol{\tau}} = \tilde{\boldsymbol{\tau}}(\mathbf{x}_R)$, which was previously developed in [5] and stabilizes $\mathbf{x}_R = \mathbf{0}$ almost globally asymptotically.

The translational tracking error is

$$\mathbf{x}_p = \begin{bmatrix} \tilde{\mathbf{p}} \\ \dot{\tilde{\mathbf{p}}} \end{bmatrix} = \begin{bmatrix} \mathbf{p}_I - \mathbf{p}_{d,I} \\ \dot{\mathbf{p}}_I - \dot{\mathbf{p}}_{d,I} \end{bmatrix} \in \mathbb{R}^6 . \tag{17}$$

By choosing the desired thrust force

$$\mathbf{F}_{d,I} = F_d \cdot (-\mathbf{z}_{d,I}) = \mathbf{D}\dot{\mathbf{p}}_{d,I} - mg\mathbf{e}_z + m\ddot{\mathbf{p}}_{d,I} + \tilde{\mathbf{F}} \tag{18}$$

and using (6) the translational tracking error dynamics read

$$\dot{\mathbf{x}}_p = \underbrace{\begin{bmatrix} \dot{\tilde{\mathbf{p}}} \\ -\frac{1}{m}\mathbf{D}\dot{\tilde{\mathbf{p}}} + \frac{1}{m}\tilde{\mathbf{F}} \end{bmatrix}}_{\mathbf{f}_p(\mathbf{x}_p, \tilde{\mathbf{F}})} + \underbrace{\begin{bmatrix} \mathbf{0} \\ \frac{1}{m}(F_d\mathbf{z}_{d,I} - F\mathbf{z}_I) \end{bmatrix}}_{\mathbf{g}_p}, \tag{19}$$

where $\mathbf{g}_p$ is the acceleration caused by the difference between the desired and the current thrust force. In Section 6 we will develop a partial-feedback control law $\tilde{\mathbf{F}} = \tilde{\mathbf{F}}(\mathbf{x}_p)$, such that $\mathbf{x}_p = \mathbf{0}$ is an asymptotically stable equilibrium of $\dot{\mathbf{x}}_p = \mathbf{f}_p(\mathbf{x}_p, \tilde{\mathbf{F}}(\mathbf{x}_p))$. If moreover $\mathbf{g}_p = \mathbf{0}$ holds when $\mathbf{z}_I = \mathbf{z}_{d,I}$, one may expect that guaranteeing asymptotic tracking of the desired attitude will guarantee tracking of $\mathbf{p}_d$. In Section 5 we will show that this holds true if some additional conditions are fulfilled.

The vector $\mathbf{g}_p$ couples the attitude tracking error dynamics (10), (11) with the translational tracking error dynamics (19). We will now briefly clarify how $\mathbf{g}_p$ relates to the error states $\mathbf{x}_R$ and $\mathbf{x}_p$ and how it relates to the reference inputs $\mathbf{p}_{d,I}$ and $\mathbf{h}_{d,I}$. Since we choose $\tilde{\mathbf{F}} = \tilde{\mathbf{F}}(\mathbf{x}_p)$, it follows for the desired thrust force (18) that $\mathbf{F}_{d,I} = \mathbf{F}_{d,I}(\tilde{\mathbf{F}}(\mathbf{x}_p), \dot{\mathbf{p}}_{d,I}, \ddot{\mathbf{p}}_{d,I})$ holds. Considering that $F_d = \|\mathbf{F}_{d,I}\|$ and $\mathbf{z}_{d,I} = -\mathbf{F}_{d,I}/\|\mathbf{F}_{d,I}\|$ it follows for the magnitude of the desired thrust force

$$F_d = F_d(\tilde{\mathbf{F}}(\mathbf{x}_p), \dot{\mathbf{p}}_{d,I}, \ddot{\mathbf{p}}_{d,I}) \tag{20}$$

and for the desired z-axis direction

$$\mathbf{z}_{d,I} = \mathbf{z}_{d,I}(\tilde{\mathbf{F}}(\mathbf{x}_p), \dot{\mathbf{p}}_{d,I}, \ddot{\mathbf{p}}_{d,I}) . \tag{21}$$

Furthermore, the actual z-axis direction $\mathbf{z}_I$ is given by $\mathbf{z}_I = \mathbf{R}_{ID}\mathbf{R}_{BD}^T\mathbf{e}_z$. The matrix $\mathbf{R}_{ID}$ contained in this equation is a function of $\mathbf{h}_{d,I}$ and $\mathbf{z}_{d,I}$, i. e.

$$\mathbf{R}_{ID} = \mathbf{R}_{ID}(\mathbf{h}_{d,I}, \mathbf{z}_{d,I}) . \tag{22}$$

This can be seen by using the fact that $\mathbf{R}_{ID} = \begin{bmatrix} \mathbf{x}_{d,I} & \langle\!\langle \mathbf{z}_{d,I} \rangle\!\rangle \mathbf{x}_{d,I} & \mathbf{z}_{d,I} \end{bmatrix}$ and that according to (9) we have

$$\mathbf{x}_{d,I} = \mathbf{x}_{d,I}(\mathbf{h}_{d,I}, \mathbf{z}_{d,I}) . \tag{23}$$

Moreover, by concluding from (14) that $\mathbf{R}_{BD} = \mathbf{R}_{BD}(\mathbf{x}_R)$ and using (21) one deduces for $\mathbf{z}_I$ that

$$\mathbf{z}_I = \mathbf{z}_I(\tilde{\mathbf{F}}(\mathbf{x}_p), \mathbf{x}_R, \dot{\mathbf{p}}_{d,I}, \ddot{\mathbf{p}}_{d,I}, \mathbf{h}_{d,I}) \tag{24}$$

holds. Finally, by restricting us to thrust control laws of the form

$$F = k_F(\mathbf{x}_R) \cdot F_d \tag{25}$$

one can infer from (20), (21), (24) and (25) that

$$\mathbf{g}_p = \mathbf{g}_p(\tilde{\mathbf{F}}(\mathbf{x}_p), k_F(\mathbf{x}_R), \mathbf{x}_R, \dot{\mathbf{p}}_{d,I}, \ddot{\mathbf{p}}_{d,I}, \mathbf{h}_{d,I}) \tag{26}$$

applies.

Remark 1. The desired z-axis direction $\mathbf{z}_{d,I} = -\mathbf{F}_{d,I}/\|\mathbf{F}_{d,I}\|$ is only well defined if $\|\mathbf{F}_{d,I}\| \neq 0$ holds. It follows from (18) that this can be guaranteed if

$$\|\mathbf{D}\dot{\mathbf{p}}_{d,I} + m\ddot{\mathbf{p}}_{d,I} + \tilde{\mathbf{F}}\| < mg \tag{27}$$

is ensured. In Section 6 we develop a control law $\tilde{\mathbf{F}}(\mathbf{x}_p)$, which satisfies $\|\tilde{\mathbf{F}}\| < \bar{F}$ for a given bound $\bar{F}$. By designing the desired position trajectory $\mathbf{p}_d(t)$ such that $\|\mathbf{D}\dot{\mathbf{p}}_{d,I} + m\ddot{\mathbf{p}}_{d,I}\| < mg - \bar{F}$ holds, compliance with (27) is guaranteed. Note that (27) also ensures that $\mathbf{z}_{d,I}$ can never lie within the horizontal plane and accordingly the normalized projection (9) is always well defined.

Remark 2. In order to render the control torque $\boldsymbol{\tau}$ continuous, the desired trajectories $\mathbf{p}_{d,I}(t)$, $\mathbf{h}_{d,I}(t)$ as well as the control laws $\tilde{\mathbf{F}}(\mathbf{x}_p)$ and $k_F(\mathbf{x}_R)$ have to satisfy some smoothness conditions. The strongest smoothness requirements arise from the term $\dot{\boldsymbol{\omega}}_B^{ID}$ in (15). To guarantee continuity of $\dot{\boldsymbol{\omega}}_B^{ID}$, according to (13) continuity of $\ddot{\mathbf{R}}_{ID}$ is required. Since in view of (22) it holds that $\ddot{\mathbf{R}}_{ID} = \ddot{\mathbf{R}}_{ID}(\mathbf{h}_{d,I}, \dot{\mathbf{h}}_{d,I}, \ddot{\mathbf{h}}_{d,I}, \mathbf{z}_{d,I}, \dot{\mathbf{z}}_{d,I}, \ddot{\mathbf{z}}_{d,I})$ we certainly need continuity of the arguments, which leads us to the following smoothness conditions:

- Continuity of the argument $\ddot{\mathbf{h}}_{d,I}$ requires $\mathbf{h}_{d,I}(t) \in C^2$.
- Starting from (21), one concludes that $\mathbf{p}_{d,I}(t) \in C^4$ and $\tilde{\mathbf{F}}(\mathbf{x}_p) \in C^2$ is necessary to guarantee continuity of $\ddot{\mathbf{z}}_{d,I} = \ddot{\mathbf{z}}_{d,I}(\tilde{\mathbf{F}}, \dot{\tilde{\mathbf{F}}}, \ddot{\tilde{\mathbf{F}}}, \dot{\mathbf{p}}_{d,I}, \ddot{\mathbf{p}}_{d,I}, \mathbf{p}_{d,I}^{(3)}, \mathbf{p}_{d,I}^{(4)})$.
- Moreover, continuity of $\ddot{\mathbf{z}}_{d,I}$ requires a continuous $\ddot{\tilde{\mathbf{F}}} = \ddot{\tilde{\mathbf{F}}}(\mathbf{x}_p, \dot{\mathbf{x}}_p, \ddot{\mathbf{x}}_p)$ and consequently a continuous $\ddot{\mathbf{x}}_p$. It follows from (19) that $\ddot{\mathbf{x}}_p = \ddot{\mathbf{x}}_p(\mathbf{x}_p, \dot{\mathbf{x}}_p, \tilde{\mathbf{F}}, \dot{\tilde{\mathbf{F}}}, \mathbf{g}_p, \dot{\mathbf{g}}_p)$ and based on (26) we finally deduce $\dot{\mathbf{g}}_p = \dot{\mathbf{g}}_p(\tilde{\mathbf{F}}, \dot{\tilde{\mathbf{F}}}, k_F, \dot{k}_F, \mathbf{x}_R, \dot{\mathbf{x}}_R, \dot{\mathbf{p}}_{d,I}, \ddot{\mathbf{p}}_{d,I}, \dot{\mathbf{p}}_{d,I}^{(3)}, \mathbf{h}_{d,I}, \dot{\mathbf{h}}_{d,I})$. Accordingly, $k_F(\mathbf{x}_R) \in C^1$ must hold.

5 Stability properties of the cascade system

The position tracking error dynamics (19) and the attitude tracking error dynamics (16) form a cascade system

$$\dot{\mathbf{x}}_p = \mathbf{f}_p(\mathbf{x}_p, \tilde{\mathbf{F}}(\mathbf{x}_p)) + \mathbf{g}_p(\mathbf{x}_p, \mathbf{x}_R, \mathbf{d}) \tag{28a}$$

$$\dot{\mathbf{x}}_R = \mathbf{f}_R(\mathbf{x}_R, \tilde{\boldsymbol{\tau}}(\mathbf{x}_R))\,, \tag{28b}$$

where $\mathbf{d} = \begin{bmatrix}\dot{\mathbf{p}}_{d,I}^T & \ddot{\mathbf{p}}_{d,I}^T & \mathbf{h}_{d,I}^T\end{bmatrix}^T$ is an exogenous input.

For the remainder of this section we consider a general nonlinear cascade system of the form (28), where $\mathbf{f}_p(\mathbf{x}_p, \tilde{\mathbf{F}}(\mathbf{x}_p))$ is a locally Lipschitz vector field on $\mathbb{R}^{n_p}$ satisfying $\mathbf{f}_p(\mathbf{0}, \tilde{\mathbf{F}}(\mathbf{0})) = \mathbf{0}$ and $\mathbf{f}_R(\mathbf{x}_R, \tilde{\boldsymbol{\tau}}(\mathbf{x}_R))$ is a locally Lipschitz vector field on the smooth manifold $\mathcal{M} \subseteq \mathbb{R}^{n_R}, \mathbf{0} \in \mathcal{M}$ satisfying $\mathbf{f}_R(\mathbf{0}, \tilde{\boldsymbol{\tau}}(\mathbf{0})) = \mathbf{0}$. The function $\mathbf{g}_p(\mathbf{x}_p, \mathbf{x}_R, \mathbf{d})$ is assumed to be continuous in its arguments. In the following we will present sufficient conditions for asymptotic stability (AS) of $(\mathbf{x}_p, \mathbf{x}_R) = (\mathbf{0}, \mathbf{0})$.

The stability of cascade systems has been studied in numerous publications under different assumptions, none of which exactly match our problem. See [18] for a brief literature review. The majority of the classical results like e. g. [10, 20, 25–27] is concerned with autonomous systems and hence not applicable to our problem, since the interconnection term in (28a) depends on the exogenous input $\mathbf{d}$ and accordingly (28) is time-varying. In [22] and more detailed in [18] time-varying cascades are considered, but the results are mainly tailored for an interconnection term of the form $\mathbf{g}_p = \mathbf{g}(t, \mathbf{x}_p, \mathbf{x}_R)\,\mathbf{x}_R$, which does not hold in our case. Moreover, the analysis is restricted to cascades of subsystems with global stability properties. We in contrast will analyze the cascade considering that the stability properties of $\mathbf{x}_R = \mathbf{0}$ in (28b) may be only local and we will show that its region of attraction propagates to the region of attraction of the whole cascade. Similar as in [2] we derive our result by adapting the findings from [27] and [26] based on the following assumptions:

Assumption 1 (Subsystem stability). *The equilibrium $\mathbf{x}_p = \mathbf{0}$ of $\dot{\mathbf{x}}_p = \mathbf{f}_p(\mathbf{x}_p, \tilde{\mathbf{F}}(\mathbf{x}_p))$ is globally asymptotically stable (GAS) and the equilibrium $\mathbf{x}_R = \mathbf{0}$ of $\dot{\mathbf{x}}_R = \mathbf{f}_R(\mathbf{x}_R, \tilde{\boldsymbol{\tau}}(\mathbf{x}_R))$ is locally exponentially stable (LES) with region of attraction $\mathcal{A}_R$.*

Assumption 2 (Growth restriction on $\mathbf{g}_p$). *There exists a class $\mathcal{K}$ function $\gamma(\|\mathbf{x}_R\|)$, differentiable at $\|\mathbf{x}_R\| = \mathbf{0}$, such that*

$$\|\mathbf{g}_p(\mathbf{x}_p, \mathbf{x}_R, \mathbf{d})\| \leq \gamma(\|\mathbf{x}_R\|)\,. \tag{29}$$

Assumption 3 (Growth restriction on V_p). *There exist a positive semidefinite radially unbounded function $V_p(\mathbf{x}_p)$ satisfying $V_p(\mathbf{0}) = 0$ and positive constants c_1 and c_2 such that for $\|\mathbf{x}_p\| \geq c_1$*

$$\frac{\partial V_p}{\partial \mathbf{x}_p}\mathbf{f}_p(\mathbf{x}_p, \tilde{\mathbf{F}}(\mathbf{x}_p)) \leq 0\,, \tag{30}$$

$$\left\|\frac{\partial V_p}{\partial \mathbf{x}_p}\right\| \leq c_2 \cdot V_p(\mathbf{x}_p)\,. \tag{31}$$

Theorem 1 (Stability of the cascade system). *If Assumptions 1–3 are fulfilled, then the equilibrium $(\mathbf{x}_p, \mathbf{x}_R) = (\mathbf{0}, \mathbf{0})$ of the cascade system (28) is asymptotically stable with region of attraction $\mathbb{R}^{n_p} \times \mathcal{A}_R$.*

Proof. The proof comprises two steps. First, we prove that every solution with initial point in $\mathbb{R}^{n_p} \times \mathcal{A}_R$ is bounded similar as in [26][Theorem 4.7]. Based on the boundedness, we show in a second step that the origin is attractive and stable using the converging input converging state (CICS) property introduced in [27] and generalized more recently in [28]. Throughout the proof we assume $(\mathbf{x}_p(0), \mathbf{x}_R(0))$ to be any initial condition in $\mathbb{R}^{n_p} \times \mathcal{A}_R$ and we restrict the analysis to forward time, i. e. $t \in \mathbb{R}_{\geq 0}$.

For $\|\mathbf{x}_p\| \geq c_1$ it follows from Assumptions 3 and 2 that

$$\begin{aligned}\dot{V}_p &= \frac{\partial V_p}{\partial \mathbf{x}_p}\mathbf{f}_p(\mathbf{x}_p, \tilde{\mathbf{F}}(\mathbf{x}_p)) + \frac{\partial V_p}{\partial \mathbf{x}_p}\mathbf{g}_p(\mathbf{x}_p, \mathbf{x}_R, \mathbf{d}) \\ &\leq \frac{\partial V_p}{\partial \mathbf{x}_p}\mathbf{g}_p(\mathbf{x}_p, \mathbf{x}_R, \mathbf{d}) \leq \left\|\frac{\partial V_p}{\partial \mathbf{x}_p}\right\| \|\mathbf{g}_p(\mathbf{x}_p, \mathbf{x}_R, \mathbf{d})\| \\ &\leq \left\|\frac{\partial V_p}{\partial \mathbf{x}_p}\right\| \gamma(\|\mathbf{x}_R\|)\,.\end{aligned} \tag{32}$$

From the differentiability of $\gamma(\|\mathbf{x}_R\|)$ at $\|\mathbf{x}_R\| = \mathbf{0}$ it immediately follows the existence of a $c_3 > 0$ and a neighborhood $\|\mathbf{x}_R\| < \epsilon_1$ where

$$\gamma(\|\mathbf{x}_R\|) < c_3\|\mathbf{x}_R\|\,. \tag{33}$$

From the LES of $\mathbf{x}_R = \mathbf{0}$ in turn it follows the existence of a positive constant α and a continuous function $h : \mathcal{A}_R \to \mathbb{R}_{\geq 0}$, satisfying $h(\mathbf{0}) = 0$ and $h \to \infty$ for $\mathbf{x}_R \to \partial\mathcal{A}_R$, such that

$$\|\mathbf{x}_R(t)\| \leq h(\mathbf{x}_R(0))e^{-\alpha t} \quad \forall t\,. \tag{34}$$

Accordingly, for all times greater than the time

$$T(\mathbf{x}_R(0)) = \max\left(0, -\frac{1}{\alpha}\ln\left(\frac{\epsilon_1}{h(\mathbf{x}_R(0))}\right)\right) \tag{35}$$

it holds that $\|\mathbf{x}_R\| < \epsilon_1$. Consequently, the inequalities

$$\begin{aligned}\gamma(\|\mathbf{x}_R(t)\|) &\leq \gamma(h(\mathbf{x}_R(0)))e^{\alpha T(\mathbf{x}_R(0))}e^{-\alpha t} && \forall t \leq T \\ \gamma(\|\mathbf{x}_R(t)\|) &< c_3\, h(\mathbf{x}_R(0))e^{-\alpha t} && \forall t > T\end{aligned} \tag{36}$$

hold. Defining the continuous function $C : \mathcal{A}_R \to \mathbb{R}_{\geq 0}$,

$$C(\mathbf{x}_R) = \max\left(\gamma(h(\mathbf{x}_R))e^{\alpha T(\mathbf{x}_R)}, c_3\, h(\mathbf{x}_R)\right), \tag{37}$$

which satisfies $C(\mathbf{0}) = 0$ and $C \to \infty$ for $\mathbf{x}_R \to \partial\mathcal{A}_R$, finally leads to

$$\gamma(\|\mathbf{x}_R(t)\|) \leq C(\mathbf{x}_R(0))e^{-\alpha t} \quad \forall t\,. \tag{38}$$

Inserting this into (32) and using (31) yields

$$\dot{V}_p \leq \left\|\frac{\partial V_p}{\partial \mathbf{x}_p}\right\| C(\mathbf{x}_R(0))e^{-\alpha t} \leq c_2\, C(\mathbf{x}_R(0))e^{-\alpha t}\, V_p \tag{39}$$

for $\|\mathbf{x}_p(t)\| \geq c_1$. From this estimate the boundedness of $V_p(\mathbf{x}_p(t))$ directly follows, since as long as $\|\mathbf{x}_p(t)\| \geq c_1$ it holds that

$$\begin{aligned} V_p(\mathbf{x}_p(t)) &\leq \bar{V}_p(\mathbf{x}_p(0))e^{\int_0^t c_2\, C(\mathbf{x}_R(0))e^{-\alpha s}ds} \\ &\leq \bar{V}_p(\mathbf{x}_p(0))e^{c_2\, C(\mathbf{x}_R(0))\frac{1}{\alpha}}\,, \end{aligned} \tag{40}$$

where

$$\bar{V}_p(\mathbf{x}_p(0)) = \max\left(V_p(\mathbf{x}_p(0)), \max_{\|\mathbf{x}_p\|=c_1} V_p(\mathbf{x}_p)\right). \tag{41}$$

Because $V_p(\mathbf{x}_p)$ is radially unbounded, the boundedness of $V_p(\mathbf{x}_p(t))$ implies the boundedness of $\|\mathbf{x}_p(t)\|$ for $\|\mathbf{x}_p(t)\| \geq c_1$. If $\|\mathbf{x}_p(t)\| < c_1$ the boundedness is trivially fulfilled.

In a second step, we now deduce asymptotic stability of $(\mathbf{x}_p, \mathbf{x}_R) = (\mathbf{0}, \mathbf{0})$. First, we consider $\mathbf{g}_p$ in (28a) as an input,

$$\dot{\mathbf{x}}_p = \tilde{\mathbf{f}}_p(\mathbf{x}_p, \tilde{\mathbf{F}}(\mathbf{x}_p), \mathbf{g}_p)\,. \tag{42}$$

According to Assumption 1, the equilibrium $\mathbf{x}_p = \mathbf{0}$ of the system $\dot{\mathbf{x}}_p = \tilde{\mathbf{f}}_p(\mathbf{x}_p, \tilde{\mathbf{F}}(\mathbf{x}_p), \mathbf{0})$ is GAS. It is known from [27] that in this case there exists a smooth function $\beta(\mathbf{x}_p) \neq 0,\ \forall \mathbf{x}_p$, such that the system

$$\dot{\mathbf{x}}_p = \tilde{\mathbf{f}}_p(\mathbf{x}_p, \tilde{\mathbf{F}}(\mathbf{x}_p), \beta(\mathbf{x}_p)\mathbf{v}) \tag{43}$$

is CICS with respect to the new input $\mathbf{v}$. Due to Assumption 1 and (29), the interconnection term $\mathbf{g}_p$ is bounded and boundedness of $\|\mathbf{x}_p\|$ was proven before. It follows that there exists an input

$$\mathbf{v} = \frac{\mathbf{g}_p}{\beta(\mathbf{x}_p)} \tag{44}$$

such that the solutions of (42) and (43) are the same. As $\lim_{t\to\infty} \mathbf{x}_R(t) = \mathbf{0}$ and $\mathbf{g}_p(\mathbf{x}_p, \mathbf{0}, \mathbf{d}) = \mathbf{0}$, it holds that $\lim_{t\to\infty} \mathbf{g}_p(t) = \mathbf{0}$ and consequently $\lim_{t\to\infty} \mathbf{v}(t) = \mathbf{0}$. It then follows from the CICS property that $\lim_{t\to\infty} \mathbf{x}_p(t) = \mathbf{0}$ and consequently $(\mathbf{x}_p, \mathbf{x}_R) = (\mathbf{0}, \mathbf{0})$ is attractive.

Furthermore, it is known from [27] that the CICS property of (43) guarantees the existence of constants $\delta_p > 0$ and $v_{max} > 0$ such that for any $\epsilon_2 > 0$

$$\|\mathbf{x}_p(t)\| < \epsilon_2 \quad \forall t \tag{45}$$

if $\|\mathbf{x}_p(0)\| < \delta_p$ and $\|\mathbf{v}(t)\| < v_{max}$ holds for all times. By defining

$$\beta_{min} = \inf_{\|\mathbf{x}_p\|<\epsilon_2} |\beta(\mathbf{x}_p)|\,, \tag{46}$$

it follows from (44) that for any v_{max} there exists a $g_{max} = \beta_{min} v_{max} > 0$ such that $\|\mathbf{v}(t)\| < v_{max}$ is always guaranteed if $\|\mathbf{g}_p(t)\| < g_{max}$ holds for all times. AS of $\mathbf{x}_R = \mathbf{0}$ and (29) in turn ensure that for any g_{max} there exists a constant $\delta_R > 0$ such that $\|\mathbf{g}_p(t)\| < g_{max}$ is valid for all times if the initial condition satisfies $\|\mathbf{x}_R(0)\| < \delta_R$. Stability of $(\mathbf{x}_p, \mathbf{x}_R) = (\mathbf{0}, \mathbf{0})$ directly follows. □

According to Theorem 1, any overall control which consists of a position control law $\tilde{\mathbf{F}}(\mathbf{x}_p)$, a thrust control law $F = k_F(\mathbf{x}_R) \cdot F_d$ and an attitude control law $\tilde{\boldsymbol{\tau}}(\mathbf{x}_R)$, and which leads to compliance with Assumptions 1-3, will solve the tracking control problem formulated in Section 3. The following sections are devoted to the development of such an overall control law.

Remark 3. Let us consider some aspects concerning the conservatism of the Assumptions 1–3. Certainly, the LES requirement of Assumption 1 will be satisfied in most cases, since it is equivalent to AS of the linearization. The majority of well-established control approaches lead to systems with an AS linearization. Clearly, the GAS requirement of Assumption 1 is more restrictive and will not be satisfiable for any system, especially if the control variables are constrained. The influence of the Assumptions 2 and 3 is more involved. While (30) simply states that for $\|\mathbf{x}_p\| \geq c_1$ the function V_p acts like a Lyapunov function for the subsystem $\dot{\mathbf{x}}_p = \mathbf{f}_p(\mathbf{x}_p, \tilde{\mathbf{F}}(\mathbf{x}_p))$, there is a tradeoff between the growth restrictions (29) and (31). It was discussed in [18] that the growth restriction on the coupling term (29) can be relaxed, if in return the growth restriction on the V_p (31) is strengthened and vice versa. Of course this may help us to find a suitable growth condition for the coupling term in question, but makes it more complicated (or even impossible) to find a suitable function V_p. On the other hand, quite intuitive control approaches may sometimes (like in the quadrotor case) lead directly to compliance with all assumptions.

6 Position control loop

In this section we develop a position control law $\tilde{\mathbf{F}}(\mathbf{x}_p)$ for the simplified system $\dot{\mathbf{x}}_p = \mathbf{f}_p(\mathbf{x}_p, \tilde{\mathbf{F}})$, which neglects the interconnection term $\mathbf{g}_p$ present in the original position tracking error dynamics (19). The control law is designed using energy shaping and damping injection techniques as presented e. g. in [21]. This means constructing the controller such that the closed loop system obeys an appropriate energy function V_p, which has a strict minimum at the desired operating point $\mathbf{x}_p = \mathbf{0}$.

Let us consider a continuously differentiable, radially unbounded function

$$V_p(\mathbf{x}_p) = E_{kin}(\dot{\tilde{\mathbf{p}}}) + E_{pot}(\tilde{\mathbf{p}}) = \frac{1}{2} m \dot{\tilde{\mathbf{p}}}^T \dot{\tilde{\mathbf{p}}} + E_{pot}(\tilde{\mathbf{p}}) \quad (47)$$

which consists of a kinetic and a potential energy part and satisfies $V_p(\mathbf{0}) = 0$ and $V_p(\mathbf{x}_p) > 0$ in $\mathbb{R}^{n_p} \backslash \{\mathbf{0}\}$. Taking the time derivative of V_p with respect to the simplified dynamics yields

$$\dot{V}_p(\mathbf{x}_p) = m \dot{\tilde{\mathbf{p}}}^T \ddot{\tilde{\mathbf{p}}} + \dot{E}_{pot} = -\dot{\tilde{\mathbf{p}}}^T \mathbf{D} \dot{\tilde{\mathbf{p}}} + \dot{\tilde{\mathbf{p}}}^T \tilde{\mathbf{F}} - \mathbf{F}_{pot}^T \dot{\tilde{\mathbf{p}}}, \quad (48)$$

where $\mathbf{F}_{pot}(\tilde{\mathbf{p}}) = -(\partial E_{pot}/\partial \tilde{\mathbf{p}})^T$ can be identified as the force resulting from the potential energy E_{pot}. It follows, that the application of a control input of the form

$$\tilde{\mathbf{F}}(\mathbf{x}_p) = \mathbf{F}_{pot}(\tilde{\mathbf{p}}) - \mathbf{D}_{\tilde{\mathbf{F}}}(\mathbf{x}_p) \dot{\tilde{\mathbf{p}}}, \quad (49)$$

where $\mathbf{D}_{\tilde{\mathbf{F}}} > 0$ is a damping matrix, leads to $\dot{V} \leq 0$ and thus is suitable for the stabilization of $\mathbf{x}_p = \mathbf{0}$.

Accordingly, the controller is designed in two steps. First the total energy V_p is shaped by designing a suitable potential energy function E_{pot}. This determines $\mathbf{F}_{pot}$, which is the first component of the control law. The second step is the damping injection stage, which defines the second component of the control law. It consists of finding an appropriate damping matrix $\mathbf{D}_{\tilde{\mathbf{F}}} > 0$ to control the energy dissipation in the system.

Theorem 2. *Consider the system* $\dot{\mathbf{x}}_p = \mathbf{f}_p(\mathbf{x}_p, \tilde{\mathbf{F}})$ *with* $\mathbf{f}_p(\mathbf{x}_p, \tilde{\mathbf{F}})$ *given in* (19) *and an energy function* V_p *as in* (47). *The control law* (49) *globally stabilizes* $\mathbf{x}_p = \mathbf{0}$. *If moreover* E_{pot} *has no critical points apart from* $\tilde{\mathbf{p}} = \mathbf{0}$ *the origin* $\mathbf{x}_p = \mathbf{0}$ *is GAS.*

Proof. Inserting (49) into (48) yields

$$\dot{V}_p(\mathbf{x}_p) = \frac{\partial V_p}{\partial \mathbf{x}_p} \mathbf{f}_p(\mathbf{x}_p, \tilde{\mathbf{F}}(\mathbf{x}_p)) = -\dot{\tilde{\mathbf{p}}}^T (\mathbf{D} + \mathbf{D}_{\tilde{\mathbf{F}}}) \dot{\tilde{\mathbf{p}}} \leq 0. \quad (50)$$

Hence, V_p is a Lyapunov function and global stability of $\mathbf{x}_p = \mathbf{0}$ follows. Applying LaSalle's invariance principle (see e. g. [12][Theorem 4.4]) we conclude that all closed loop trajectories converge to the largest invariant set contained in $\mathcal{E} = \{\mathbf{x}_p : \dot{V}_p(\mathbf{x}_p) = 0 \Leftrightarrow \dot{\tilde{\mathbf{p}}} = \mathbf{0}\}$. For all $\mathbf{x}_p \in \mathcal{E}$ it holds that $\ddot{\tilde{\mathbf{p}}} = 1/m \cdot \mathbf{F}_{pot}$ and consequently the largest invariant subset is given by all points satisfying $\ddot{\tilde{\mathbf{p}}} = 1/m \cdot \mathbf{F}_{pot} = \mathbf{0} \Leftrightarrow \mathbf{F}_{pot} = \mathbf{0}$. Since $\mathbf{F}_{pot}(\tilde{\mathbf{p}}) = -(\partial E_{pot}/\partial \tilde{\mathbf{p}})^T$ holds this invariant set reduces to $\mathbf{x}_p = \mathbf{0}$ if E_{pot} has no critical points apart from $\mathbf{x}_p = \mathbf{0}$. This proves GAS of $\mathbf{x}_p = \mathbf{0}$. □

In the following subsections the potential energy E_{pot} and the damping matrix $\mathbf{D}_{\tilde{\mathbf{F}}}$ are designed such that the following properties hold:

- P1 $\mathbf{x}_p = \mathbf{0}$ is GAS, according to Theorem 2.
- P2 There exist positive constants c_1 and c_2 such that for $\|\mathbf{x}_p(t)\| \geq c_1$ the function V_p fulfills $\left\| \frac{\partial V_p}{\partial \mathbf{x}_p} \right\| \leq c_2 \cdot V_p(\mathbf{x}_p)$.
- P3 $\|\tilde{\mathbf{F}}\| < \bar{F}$, where $\bar{F} > 0$ is a given bound.
- P4 $\tilde{\mathbf{F}}(\mathbf{x}_p) \in C^2$.

Note that it follows from P1 that (50) holds. This together with P2 ensures that Assumption 3 is fulfilled. The benefit of P3 has been addressed in Remark 1 and the necessity of P4 has been discussed in Remark 2.

6.1 Shaping of the potential energy

The shape of the potential energy determines the first component $\mathbf{F}_{pot}$ of the control law (49). Introducing the two positive constants $\bar{r}$, $c_r < \bar{F}/\bar{r}$ and using the saturation function $\bar{\sigma}^{\bar{a}}_{\Delta_a}$ defined in (2), we assign the circular and radially unbounded potential energy function

$$E_{pot}(\tilde{\mathbf{p}}) = \int_0^{\|\tilde{\mathbf{p}}\|} c_r \, \bar{\sigma}^{\bar{r}}_{\Delta_r}(s) \, ds \quad (51)$$

to the closed loop system. Accordingly, we obtain

$$\mathbf{F}_{pot}(\tilde{\mathbf{p}}) = -\left(\frac{\partial E_{pot}}{\partial \tilde{\mathbf{p}}} \right)^T = -c_r \, \bar{\sigma}^{\bar{r}}_{\Delta_r}(\|\tilde{\mathbf{p}}\|) \frac{1}{\|\tilde{\mathbf{p}}\|} \tilde{\mathbf{p}}, \quad (52)$$

where c_r, $\bar{r}$ and Δ_r are the design parameters. Provided that $\Delta_r < \bar{r}$ one can easily verify that $\mathbf{F}_{pot}$ behaves like the force of linear spring with stiffness coefficient c_r near $\tilde{\mathbf{p}} = \mathbf{0}$, i. e. $\mathbf{F}_{pot} = -c_r \tilde{\mathbf{p}}$. With increasing $\|\tilde{\mathbf{p}}\|$ it then saturates to the value $c_r \bar{r}$, which has to satisfy $c_r \bar{r} < \bar{F}$ to comply with property P3. Note that $\mathbf{F}_{pot} = \mathbf{0}$ holds only for $\tilde{\mathbf{p}} = \mathbf{0}$ and accordingly this is the only critical point of E_{pot}. Consequently, GAS of $\tilde{\mathbf{p}} = \mathbf{0}$ follows from Theorem 2 by choosing any $\mathbf{D}_{\tilde{\mathbf{F}}} > 0$.

To show that V_p has Property P2, observe that

$$\begin{aligned} V_p(\mathbf{x}_p) &= \frac{1}{2} m \dot{\tilde{\mathbf{p}}}^T \dot{\tilde{\mathbf{p}}} + \int_0^{\|\tilde{\mathbf{p}}\|} c_r \, \bar{\sigma}^{\bar{r}}_{\Delta_r}(s) \, ds \\ &> \frac{1}{2} m \|\dot{\tilde{\mathbf{p}}}\|^2 + c_r \, \bar{r} \, (\|\tilde{\mathbf{p}}\| - (\bar{r} + \Delta_r)) = \underline{V}(\mathbf{y}) \,, \end{aligned} \tag{53}$$

where $\mathbf{y} = \begin{bmatrix} \|\tilde{\mathbf{p}}\| & \|\dot{\tilde{\mathbf{p}}}\| \end{bmatrix}^T$. Moreover, the inequality

$$\begin{aligned} \left\| \frac{\partial V_p}{\partial \mathbf{x}_p} \right\| &= \sqrt{\left\| c_r \, \bar{\sigma}^{\bar{r}}_{\Delta_r}(\|\tilde{\mathbf{p}}\|) \frac{1}{\|\tilde{\mathbf{p}}\|} \tilde{\mathbf{p}} \right\|^2 + m^2 \|\dot{\tilde{\mathbf{p}}}\|^2} \\ &\leq \sqrt{c_r^2 \bar{r}^2 + m^2 \|\dot{\tilde{\mathbf{p}}}\|^2} = \left\| \frac{\partial \underline{V}}{\partial \mathbf{y}} \right\| \end{aligned} \tag{54}$$

holds. Since $\underline{V}(\mathbf{y})$ is a polynomial function one concludes from the proof of [26][Proposition 4.8] [1] that there exist positive constants c_1^* and c_2 such that

$$\left\| \frac{\partial \underline{V}}{\partial \mathbf{y}} \right\| \|\mathbf{y}\| < c_2 \, \underline{V}(\mathbf{y}) \quad \forall \|\mathbf{y}\| \geq c_1^* \,. \tag{55}$$

Using $\|\mathbf{y}\| = \|\mathbf{x}_p\|$ it follows from (53), (54) and (55) that for any $\|\mathbf{x}_p\| \geq c_1 = \max(1, c_1^*)$

$$\left\| \frac{\partial V_p}{\partial \mathbf{x}_p} \right\| < \left\| \frac{\partial V_p}{\partial \mathbf{x}_p} \right\| \|\mathbf{x}_p\| \leq \left\| \frac{\partial \underline{V}}{\partial \mathbf{y}} \right\| \|\mathbf{y}\| < c_2 \, \underline{V}(\mathbf{y}) < c_2 \, V_p(\mathbf{x}_p) \tag{56}$$

holds.

6.2 Damping injection

The design of the damping matrix $\mathbf{D}_{\tilde{\mathbf{F}}}$ determines the second component $-\mathbf{D}_{\tilde{\mathbf{F}}}(\mathbf{x}_p)\dot{\tilde{\mathbf{p}}}$ of the control law (49). As mentioned above, any positive definite $\mathbf{D}_{\tilde{\mathbf{F}}}$ leads to GAS of $\tilde{\mathbf{p}} = \mathbf{0}$. We will inject a state dependent damping into the closed loop system, which pursues the following objectives. It should provide a desirable well damped behavior near the origin $\tilde{\mathbf{p}} = \mathbf{0}$, but it should omit to unnecessarily slow down the system, especially when $\|\tilde{\mathbf{p}}\| \gg 0$. Moreover, the damping will be used to guarantee Property P3.

Inserting the control law $\tilde{\mathbf{F}}(\mathbf{x}_p)$ given in (49) into the simplified system $\dot{\mathbf{x}}_p = \mathbf{f}_p(\mathbf{x}_p, \tilde{\mathbf{F}})$ yields

$$\ddot{\tilde{\mathbf{p}}} = -\frac{1}{m}(\mathbf{D} + \mathbf{D}_{\tilde{\mathbf{F}}})\dot{\tilde{\mathbf{p}}} + \frac{1}{m}\mathbf{F}_{pot} \,. \tag{57}$$

As we want to keep the damping design simple, we restrict us to positive definite, diagonal damping matrices of the form

$$\mathbf{D}_{\tilde{\mathbf{F}}} = \bar{\sigma}^1_{\Delta_{\kappa_r}}(\kappa_r) \, d_r \, \mathbf{I}_3 > 0 \,. \tag{58}$$

To further facilitate the design process we neglect the saturation function in a first step, assuming $\bar{\sigma}^1_{\Delta_{\kappa_r}}(\kappa_r) = 1$. Moreover, since the aerodynamic damping $\mathbf{D}$ is comparatively small, we assume $\mathbf{D} + \mathbf{D}_{\tilde{\mathbf{F}}} \approx \mathbf{D}_{\tilde{\mathbf{F}}}$ and additionally we restrict our considerations to radial motions, i. e. $\dot{\tilde{\mathbf{p}}} \parallel \tilde{\mathbf{p}}$. Applying all assumptions to the the dynamics (57), defining $r = \|\tilde{\mathbf{p}}\|$ and using (52) we obtain the scalar differential equation of an oscillator

$$\ddot{r} = -\frac{d_r}{m}\dot{r} - \frac{1}{m} c_r \, \bar{\sigma}^{\bar{r}}_{\Delta_r}(r) = -\frac{d_r}{m}\dot{r} - \frac{1}{m} c_{virt}(r) \, r \,, \tag{59}$$

where we regard the magnitude of the force from the potential energy $\|F_{pot}\| = c_r \, \bar{\sigma}^{\bar{r}}_{\Delta_r}(r)$ as the effect of a virtual spring with the declining nonlinear spring characteristic $c_{virt}(r) = {}^{c_r \, \bar{\sigma}^{\bar{r}}_{\Delta_r}(r)}/_{r}$. In contrast to a harmonic oscillator, here the damping ratio

$$\zeta = \frac{d_r}{2\sqrt{m c_{virt}(r)}} = \frac{d_r \sqrt{r}}{2\sqrt{m c_r \, \bar{\sigma}^{\bar{r}}_{\Delta_r}(r)}} \tag{60}$$

is not constant if d_r is chosen constant but it increases with $\sqrt{r}$ when the saturation is active. By choosing

$$d_r = 2\zeta_r \sqrt{m \frac{c_r \, \bar{\sigma}^{\bar{r}}_{\Delta_r}(r)}{r}} \,, \tag{61}$$

where $\zeta_r > 0$ is constant, we keep the damping ratio at a constant level for all r and thus omit excessive damping for $r = \|\tilde{\mathbf{p}}\| \gg 0$. Accordingly, ζ_r represents our tuning parameter concerning the damping.

To ensure that $\|\tilde{\mathbf{F}}\| < \bar{F}$ holds, we introduce κ_r, which is defined as the solution of the maximization problem

$$\kappa_r = \max_{\|\mathbf{F}_{pot} - \kappa d_r \dot{\tilde{\mathbf{p}}}\| = \bar{F}} \kappa \,, \tag{62}$$

which can be given analytically as

$$\kappa_r = \frac{\mathbf{F}_{pot}^T \dot{\tilde{\mathbf{p}}} + \sqrt{(\mathbf{F}_{pot}^T \dot{\tilde{\mathbf{p}}})^2 + (\bar{F}^2 - \|\mathbf{F}_{pot}\|^2)\|\dot{\tilde{\mathbf{p}}}\|^2}}{d_r \|\dot{\tilde{\mathbf{p}}}\|^2} \,. \tag{63}$$

Note that the solution is always positive real, because $\|\mathbf{F}_{pot}\| < \bar{F}$ holds. Since κ_r enters (58) via the saturation function $\bar{\sigma}^1_{\Delta_{\kappa_r}}(\kappa_r)$ it is moreover ensured that the damping never exceeds the value given by d_r.

One may easily verify that the control law (49) with $\mathbf{F}_{pot}$ according to (52) and a damping matrix $\mathbf{D}_{\tilde{\mathbf{F}}}$ according to (58), (61) and (63) fulfills the differentiability property P4.

1 Although $\underline{V}(\mathbf{y})$ does not fulfill all conditions of [26][Proposition 4.8], the proof still holds, if one considers that $\underline{V}(\mathbf{y})$ is not defined on $\mathbb{R}^2$ but on $\mathbb{R}^2_{\geq 0}$.

7 Thrust control law

The magnitude of the thrust force F is a control input of the system, which has a strong influence on the interconnection term $\mathbf{g}_p$. Since we apply control laws of the form $F = k_F(\mathbf{x}_R)F_d$ and the magnitude of the desired force F_d is already defined by (18) and the position control law (49), it remains to find a suitable function $k_F(\mathbf{x}_R)$ such that $\mathbf{g}_p$ fulfills Assumption 2.

The choice of $k_F(\mathbf{x}_R)$ comes down to the question how the desired thrust F_d should be propagated to the real thrust F if there is a deviation between the body's z-axis direction $\mathbf{z}$ and its desired direction $\mathbf{z}_d$. An intuitive solution to this problem is the orthogonal projection of $\mathbf{F}_d$ onto $-\mathbf{z}$. It follows that

$$F = -\mathbf{z}_B^T\mathbf{F}_{d,B} = \mathbf{z}_B^T\mathbf{z}_{d,B}\cdot F_d = \mathbf{e}_z^T\mathbf{z}_{d,B}\cdot F_d\,. \tag{64}$$

Since F cannot be negative, the projection term has to be saturated to values greater than zero. By using the thrust control law

$$F = \underline{\sigma}^{k}_{\Delta_k}(\mathbf{e}_z^T\mathbf{z}_{d,B})\cdot F_d = k_F(\mathbf{x}_R)\cdot F_d\,, \tag{65}$$

where $\underline{\sigma}^{k}_{\Delta_k}$ is the saturation function defined in (4), we bound F to values greater than $\underline{k}\cdot F_d$. Note that $\underline{k}+\Delta_k < 1$ must hold to ensure $F = F_d$ for $\mathbf{e}_z^T\mathbf{z}_{d,B} = 1$. The interested reader is referred to [2] for other admissible thrust control laws and a more detailed discussion.

It remains to show that the resulting interconnection term $\mathbf{g}_p$ is compliant with Assumption 2. Inserting (65) into the translational tracking error dynamics (19) yields

$$\begin{aligned}
\|\mathbf{g}_p\| &= \frac{F_d}{m}\|\mathbf{z}_{d,I} - k_F(\mathbf{x}_R)\mathbf{z}_I\| = \frac{F_d}{m}\|\mathbf{z}_{d,B} - k_F(\mathbf{x}_R)\mathbf{e}_z\| \\
&= \frac{F_d}{m}\|\mathbf{z}_{d,B} - \mathbf{e}_z + \mathbf{e}_z(1 - k_F(\mathbf{x}_R))\| \\
&\le \frac{F_d}{m}\left(\|\mathbf{z}_{d,B} - \mathbf{e}_z\| + |k_F(\mathbf{x}_R) - 1|\right) \\
&\le \frac{F_d}{m}\left(\|\mathbf{z}_{d,B} - \mathbf{e}_z\| + |\underline{\sigma}^{k}_{\Delta_k}(\mathbf{e}_z^T\mathbf{z}_{d,B}) - 1|\right) \\
&\le \frac{F_d}{m}\left(\|\mathbf{z}_{d,B} - \mathbf{e}_z\| + |\mathbf{e}_z^T\mathbf{z}_{d,B} - 1|\right) \\
&\le 2\frac{F_d}{m}\|\mathbf{z}_{d,B} - \mathbf{e}_z\|\,.
\end{aligned} \tag{66}$$

From (27) and (18) one concludes that $F_d < 2mg$ must hold. By noting that $\mathbf{z}_{d,B} - \mathbf{e}_z$ is the vector containing the last three elements of $\tilde{\mathbf{R}}$ it finally follows that

$$\|\mathbf{g}_p\| < 4g\|\tilde{\mathbf{R}}\| \le 4g\|\mathbf{x}_R\| = \gamma(\|\mathbf{x}_R\|)\,, \tag{67}$$

where $\gamma(\|\mathbf{x}_R\|)$ is a differentiable class $\mathcal{K}$ function.

8 Attitude control loop

The attitude control law $\tilde{\boldsymbol{\tau}}(\mathbf{x}_R)$ is taken from [5], which in turn is an extension of the quaternion based setpoint controller presented in [7]. Within this paper we will therefore restrict us to a brief recapitulation of the basic idea. Analogously to the position controller, the attitude controller is obtained by shaping an energy function

$$V_R(\mathbf{x}_R) = \frac{1}{2}(\boldsymbol{\omega}_B^{DB})^T\mathbf{J}\boldsymbol{\omega}_B^{DB} + E_R(\tilde{\mathbf{R}}) \tag{68}$$

with a strict minimum at $\mathbf{x}_R = \mathbf{0}$. Using the attitude tracking error dynamics (16), the time derivative reads

$$\dot{V}_R(\mathbf{x}_R) = (\boldsymbol{\omega}_B^{DB})^T\tilde{\boldsymbol{\tau}} + \underbrace{\frac{\partial E_R}{\partial\tilde{\mathbf{R}}}\langle\langle\tilde{\mathbf{R}} + \vec{\mathbf{I}}_3\rangle\rangle}_{-\mathbf{T}^T(\tilde{\mathbf{R}})}\boldsymbol{\omega}_B^{DB}\,, \tag{69}$$

where $\mathbf{T}$ is the torque resulting from the assigned potential energy E_R. As before, a control law

$$\tilde{\boldsymbol{\tau}} = \mathbf{T}(\tilde{\mathbf{R}}) - \mathbf{D}_{\tilde{\boldsymbol{\tau}}}(\mathbf{x}_R)\boldsymbol{\omega}_B^{DB} \tag{70}$$

is chosen, which provides the torque from the potential and injects damping $\mathbf{D}_{\tilde{\boldsymbol{\tau}}} \ge 0$ into the closed loop system. Inserting (70) into (69) yields

$$\dot{V}_R(\mathbf{x}_R) = -(\boldsymbol{\omega}_B^{DB})^T\mathbf{D}_{\tilde{\boldsymbol{\tau}}}(\mathbf{x}_R)\boldsymbol{\omega}_B^{DB} \le 0 \tag{71}$$

and stability of $\mathbf{x}_R = \mathbf{0}$ can be concluded immediately. Further properties like AS, LES and the extent of the corresponding region of attraction of the desired equilibrium depend on the specific design of the potential energy and the damping.

In [5] a suitable shaping of the closed loop energy and a sophisticated damping strategy leads to a control law that prioritizes the tracking of the desired thrust direction compared to the tracking of the heading reference. Furthermore, the controller aims at a fast transient behavior and a good exploitation of the available control authority. Since attitude control is not the focus of this paper and the expressions of the control law are rather bulky, we omit to state the equations explicitly here and refer the interested reader to [5]. Regarding the closed loop attitude tracking error dynamics, the following properties are proven in the stated reference:

P5 The zero equilibrium $\mathbf{x}_R = \mathbf{0}$ is AS and LES.

P6 The region of attraction $\mathcal{A}_R$ of $\mathbf{x}_R = \mathbf{0}$ comprises the whole state space except for a nowhere dense set of zero measure, i. e. $\mathbf{x}_R = \mathbf{0}$ is AGAS.

See [7] for some instructive simulation examples illustrating the stability properties in the setpoint case. Note that

Property P5 together with Property P1 guarantees that Assumption 1 is fulfilled.

9 Experimental results

For the validation in flight tests, the controller was implemented on an AscTec Hummingbird[2] modified for research purposes. Additionally to the basic configuration, it was equipped with an ARM Cortex-A8 processor used for the controller execution at 1 kHz. The utilized indoor test rig offered an air space of approximately 0.8 m width, 1.4 m length and 1.5 m height and provided a visual tracking system using two ceiling-mounted cameras in order to gather position and yaw angle information. Further details of the tracking system are given in [13]. The position and yaw angle data were transmitted to the quadrotor together with the reference signals at a frequency of 50 Hz. Onboard, the vision data was fused with IMU measurements to provide the complete state information. The whole process including communication, data fusion and data logging required about 30% of the available CPU power.

The experimental setup was subject to several sources of uncertainties and disturbances. The quadrotor's model parameters, which are listed in Table 1, are generally not exactly known. In particular, the aerodynamic drag matrix $\mathbf{D}$ and the moment of inertia matrix $\mathbf{J}$ are difficult to identify. While the former was roughly estimated from wind tunnel measurements, the latter has been identified through a bifilar torsional pendulum experiment. The mass m was measured directly via weighing the quadrotor in test configuration. In addition to the parameter uncertainties, the indoor environment cannot provide smooth air conditions. During flight, the rotors induce significant air flows, which act as notable disturbances on the quadrotor. Finally, the gathered sensor data, including the vision based position information, is subject to noise and measurement errors. Due to the variety of uncertainties and disturbances that have not been considered in the controller design, the presented experimental results also demonstrate the robustness of the proposed control scheme.

The set of controller parameters listed in Table 1 turned out to result in an appropriate closed loop behavior and was used for the presented flight tests. The parameters of the position and thrust controller were chosen based on the following considerations: By the choice of $\bar{F}$, the magnitude of $\tilde{\mathbf{F}}$ has been bounded to 40% of the gravity force acting on the quadrotor. This restricts the maximum tilt angle command to $0.412\,\text{rad} \approx 23.6$ in the setpoint case. The stiffness coefficient c_r has been chosen based on experience with other controllers and the bound $\bar{r}$ is chosen such that $\max(\|\mathbf{F}_{pot}\|) = c_r \cdot \bar{r} = 0.9 \cdot \bar{F} < \bar{F}$ holds. Consequently, 10% of $\bar{F}$ are available for damping purposes at all times. In view of the second order dynamics (59), the damping ratio ζ_r has been set to 0.9 to achieve a fast transient behavior with possibly minor overshoots. The value selected for $\underline{k}$ serves to saturate the projection angle of $\mathbf{F}_d$ onto $-\mathbf{z}$. Since $\underline{k} = 0.15 \approx \cos(1.420\,\text{rad})$, saturation occurs when the angle becomes greater than $1.420\,\text{rad} \approx 81.4$. Finally, the parameters Δ_r, Δ_κ and Δ_k, which determine the transition intervals of the saturation functions, were chosen empirically in accordance with the saturation limits. For the sake of completeness, the parameters of the attitude controller are also stated in Table 1. Without the explicit control law at hand, we refer to [5] and [7] for an explanatory presentation of the parameters.

Table 1: Model and controller parameters.

Model parameters	
$m = 0.585\,\text{kg}$	$g = 9.805\,\text{m/s}^2$
$\mathbf{J} = \text{diag}(6.4, 6.4, 12.5) \cdot 10^{-3}\,\text{m}^2\text{kg}$	
$\mathbf{D} = \text{diag}(0.3, 0.3, 0.3)\,\text{Ns/m}$	
Position controller parameters	
$c_r = 5.3\,\text{N/m}$	$\zeta_r = 0.9$
$\bar{r} = 0.390\,\text{m}$	$\Delta_r = 0.0390\,\text{m}$
$\bar{F} = 2.29\,\text{N}$	$\Delta_\kappa = 0.1$
Thrust control law parameters	
$\underline{k} = 0.15$	$\Delta_k = 0.05$
Attitude controller parameters (according to [5])	
$\bar{\tau}_{xy} = 0.25\,\text{Nm}$	$\bar{\tau}_z = 0.05\,\text{Nm}$
$\varphi_u = 3.11\,\text{rad}$	$\vartheta_u = 3.11\,\text{rad}$
$\varphi_l = 0.151\,\text{rad}$	$\vartheta_l = 0.426\,\text{rad}$
$c_\varphi = 1.5\,\text{Nm/rad}$	$c_\vartheta = 0.109\,\text{Nm/rad}$
$\Delta\varphi = 0.0349\,\text{rad}$	$\Delta\vartheta = 0.0349\,\text{rad}$
$\delta_\varphi = 0.176\,\text{Nms/rad}$	$\delta_\vartheta = 0.0885\,\text{Nms/rad}$
$r_\varphi = 0.75$	$r_\vartheta = 0.75$
$v_\varphi = 0.1\,\text{rad/s}$	$v_\vartheta = 0.1\,\text{rad/s}$
$v_{\varphi max} = 3.64\,\text{rad/s}$	$v_{\vartheta max} = 1.31\,\text{rad/s}$

Two test cases were chosen to demonstrate the performance of the controller: First, a periodic setpoint change in position and heading was performed and second, a three dimensional eight-shaped smooth position and a sinusoidal heading trajectory were tracked. To ease the representation of the heading in the figures, we translate the vectors $\mathbf{h}_d$ and $\mathbf{h}$ introduced in Section 3 into angle rep-

2 www.asctec.de

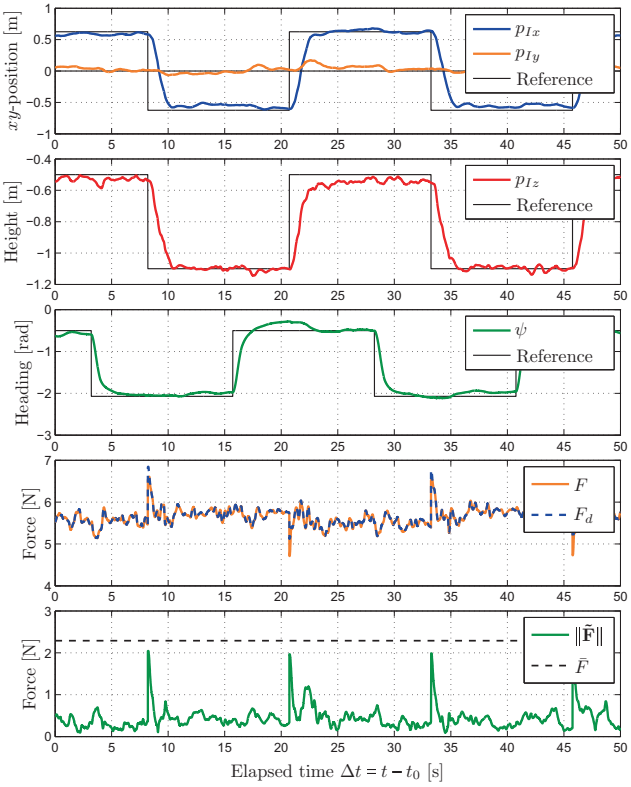

Figure 4: Results of the setpoint flight test.

resentations, defining

$$\psi_d = \text{atan2}(h_{d,Iy}, h_{d,Ix}) \quad \text{and} \quad \psi = \text{atan2}(h_{Iy}, h_{Ix}) \tag{72}$$

respectively.

The results of the setpoint changes are shown in Figure 4. The desired position $\mathbf{p}_{d,I}$ and the desired heading angle ψ_d were toggled between two constant values with a period time of 25 s. The position setpoints differed by 1.25 m in the inertial x-direction and by 0.6 m in the inertial z-direction. The desired value in the inertial y-direction was kept constantly zero. The heading command changed by $\pi/2$ rad and was phase shifted compared to the position reference. The quadrotor performed the setpoint changes fast and robustly, with no significant overshoots in the responses. Steady state errors occurred due to the aforementioned uncertainties and disturbances. Besides the position and heading responses, two plots concerning the thrust command are provided. The first shows the relation between the desired thrust F_d and the commanded thrust F. As expected from the chosen thrust control law (65), which represents a projection with saturating angle, $F \leq F_d$ always holds. The second plot shows the magnitude of the error driven component $\tilde{\mathbf{F}}$ of $\mathbf{F}_d$. According to Property P3, the magnitude $\|\tilde{\mathbf{F}}\|$ must meet the given limit value $\bar{F}$. Obviously this requirement is fulfilled at all times. Note

Table 2: Results of the setpoint flight test: Control variables.

	τ_x[Nm]	τ_y[Nm]	τ_z[Nm]	F[N]
Min. value	−0.2331	−0.2315	−0.0533	4.7120
Mean value	0.0024	−0.0049	−0.0069	5.6423
Max. value	0.3071	0.2910	0.0501	6.6067

that the peaks occur when the position reference toggles. In these moments the velocity of the quadrotor is approximately zero and accordingly almost no damping occurs. Consequently, the peaks originate almost exclusively from $\mathbf{F}_{pot}$, whose magnitude has been bounded to $0.9 \cdot \bar{F}$. Finally, Table 2 summarizes minimum, mean and maximum values of all control variables.

Although not verifiable due to the limited test rig dimensions, the controller is in principle able to handle arbitrary large position setpoint changes without endangering the system's convergence to the desired equilibrium and without the control variables growing unbounded. Moreover, the chosen bound $\bar{F}$ directly translates to a maximum desired tilt angle of the quadrotor. This is a remarkable difference to most other control concepts applied to the quadrotor.

In the second experiment the quadrotor's objective was to track the three-dimensional eight-shaped position trajectory illustrated in Figure 5 and a sinusoidal heading trajectory. Due to the limited number of uplink channels, the reference trajectories could not be transmitted together with all required time derivatives. Therefore, the reference trajectories $\mathbf{p}_{d,I}(t)$ and $\mathbf{h}_{d,I}(t)$ (and all required derivatives) were generated onboard by processing the transmitted command signals $\mathbf{p}_{c,I}(t)$ and $\psi_c(t)$. Using the fifth order filter given by the transfer function

$$G_5(s) = \frac{1}{(0.1s+1)(0.01s^2+0.22s+1)^2} \tag{73}$$

the position reference trajectory was obtained as

$$\mathbf{p}_{d,I}(s) = \text{diag}(G_5(s), G_5(s), G_5(s))\, \mathbf{p}_{c,I}(s) \tag{74}$$

and the heading reference trajectory originated from

$$\psi_d^*(s) = G_5(s)\psi_c(s) \tag{75}$$

$$\mathbf{h}_{d,I}(t) = \begin{bmatrix} \cos(\psi_d^*(t)) & \sin(\psi_d^*(t)) & 0 \end{bmatrix}^T. \tag{76}$$

Note that $\psi_d^* = \psi_d$ if $\psi_d^* \in]-\pi, \pi]$, which holds in the presented case. The transmitted command signals were

$$\mathbf{p}_{c,I}(t) = \begin{bmatrix} 0.056\,\text{m}\cdot\sin\left(\frac{\pi}{2}\frac{\text{rad}}{\text{s}}\cdot t\right) + 0.576\,\text{m}\cdot\cos\left(\frac{\pi}{4}\frac{\text{rad}}{\text{s}}\cdot t\right) \\ -0.192\,\text{m}\cdot\sin\left(\frac{\pi}{2}\frac{\text{rad}}{\text{s}}\cdot t\right) + 0.168\,\text{m}\cdot\cos\left(\frac{\pi}{4}\frac{\text{rad}}{\text{s}}\cdot t\right) \\ 0.2\,\text{m}\cdot\sin\left(\frac{\pi}{4}\frac{\text{rad}}{\text{s}}\cdot t\right) - 0.9\,\text{m} \end{bmatrix} \tag{77}$$

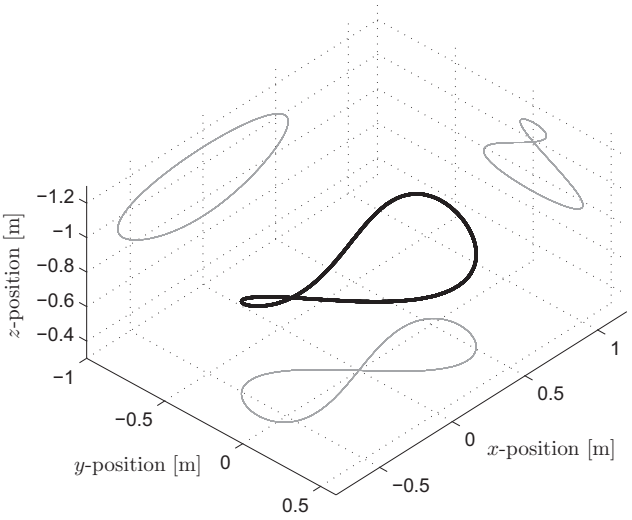

Figure 5: Perspective view of the desired trajectory $\mathbf{p}_{d,I}(t)$. Grey lines indicate projections.

Table 3: Results of the trajectory flight test: Error statistics and control variables.

	$\tilde{p}_x$ [m]	$\tilde{p}_y$ [m]	$\tilde{p}_z$ [m]	$\tilde{\psi}$ [rad]
Mean value	0.0039	0.0062	−0.0015	0.0046
Standard deviation	0.0608	0.0457	0.0257	0.0835
	τ_x [Nm]	τ_y [Nm]	τ_z [Nm]	F [N]
Min. value	−0.0901	−0.1002	−0.0351	5.1491
Mean value	0.0125	0.0040	−0.0002	5.7297
Max. value	0.1095	0.1005	0.0361	6.2222

and

$$\psi_c(t) = \frac{\pi}{4}\,\text{rad} \cdot \sin\left(\frac{\pi}{10}\frac{\text{rad}}{\text{s}} \cdot t\right) - 1.287\,\text{rad}\,. \qquad (78)$$

The position command was periodic with a period time of 8 s and the heading command's period time was 20 s. The results of the second flight test are shown in Figure 6. In order to assess the controller performance, the mean values and standard deviations of the tracking errors $\tilde{\mathbf{p}} = \begin{bmatrix}\tilde{p}_x & \tilde{p}_y & \tilde{p}_z\end{bmatrix}^T$ and $\tilde{\psi} = \psi - \psi_d$ have been computed for the presented time interval. The results are given in Table 3 and show standard deviations of maximum 6 cm in position and 0.0835 rad in heading. Regarding the external disturbances and model uncertainties the quadrotor was subject to, these values emphasize the robustness and decent performance of the presented controller architecture. For the sake of completeness, Table 3 also summarizes minimum, mean and maximum values of the control variables.

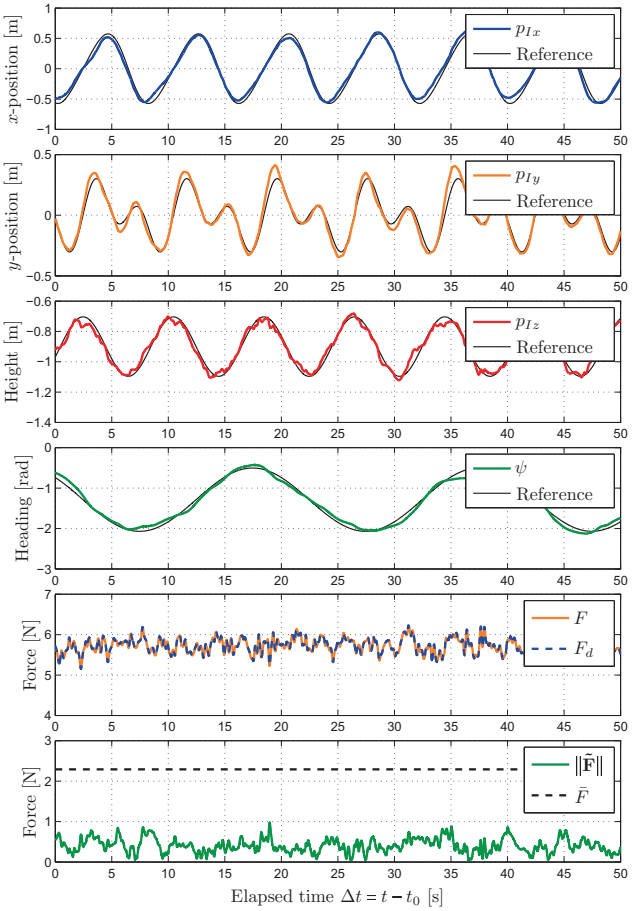

Figure 6: Results of the trajectory flight test.

10 Conclusion

Due to the cascade structure of the quadrotor dynamics, cascaded controllers represent a natural approach to solve the position and heading tracking problem. The use of cascaded controllers offers a lot of flexibility to the control engineer since the constituent controllers are designed independently for the uncoupled position and attitude subsystem using arbitrary control schemes. As time-scale separation arguments do not apply to the coupled closed loop, further considerations are required to deduce stability properties of the overall system. For a class of cascade systems including the quadrotor tracking problem, we have presented a set of assumptions which guarantee asymptotic stability of the desired equilibrium with a certain region of attraction. It was shown that these assumptions are satisfied for the presented cascaded controller which was designed using energy shaping techniques. Moreover, the position subsystem controller satisfies upper and lower bounds on the magnitude of the desired thrust force. This way the common obstacle in quadrotor control, related to

an undefined desired thrust direction when the demanded magnitude is zero, is circumvented. The suitability of the controller for practical application has been validated in experimental flight tests.

Acknowledgement: We like to thank F. Holzapfel, J. Wang and especially T. Raffler from the Institute of Flight System Dynamics of the TU München for their valuable support.

References

1. P. De Monte and B. Lohmann. Position trajectory tracking of a quadrotor based on L1 adaptive control. *at – Automatisierungstechnik*, 62(3):188–202, 2014.
2. G. Falconi, O. Fritsch, and B. Lohmann. Admissible thrust control laws for quadrotor position tracking. In *Proceedings of the American Control Conference*, pages 4844–4849, 2013.
3. I. Fantoni and R. Lozano. *Non-linear Control for Underactuated Mechanical Systems*. Springer, 2002.
4. E. Frazzoli, M. Dahleh, and E. Feron. Trajectory tracking control design for autonomous helicopters using a backstepping algorithm. In *Proceedings of the American Control Conference*, pages 4102–4107, 2000.
5. O. Fritsch. Energy based attitude tracking control for a quadrotor helicopter prioritizing the thrust direction. TRAC-7 1, Technische Universität München, 2013. https://mediatum.ub.tum.de/node?id=1160783.
6. O. Fritsch, P. De Monte, M. Buhl, and B. Lohmann. Quasi-static feedback linearization for the translational dynamics of a quadrotor helicopter. In *Proceedings of the American Control Conference*, pages 125–130, 2012.
7. O. Fritsch, B. Henze, and B. Lohmann. Fast and saturating attitude control for a quadrotor helicopter. In *Proceedings of the European Control Conference*, 2013.
8. J. Hauser, S. Sastry, and G. Meyer. Nonlinear control design for slightly non-minimum phase systems: Application to V/STOL aircraft. *Automatica*, 28(4):665–679, 1992.
9. P. Hecker, L. Bretschneider, U. Bestmann, and P. M. Schachtebeck. Flugroboter. Ein Überblick über technologische und operationelle Entwicklungen und Trends. *at – Automatisierungstechnik*, 61(4):245–258, Apr. 2013.
10. M. Jankovic, R. Sepulchre, and P. Kokotovic. Constructive Lyapunov stabilization of nonlinear cascade systems. *Automatic Control, IEEE Transactions on*, 41(12):1723–1735, 1996.
11. F. Kendoul, Z. Yu, and K. Nonamiali. Guidance and nonlinear control system for autonomous flight of minirotorcraft unmanned aerial vehicles. *Journal of Field Robotics*, 27(3):311–334, 2010.
12. H. Khalil. *Nonlinear systems*. Prentice Hall, Upper Saddle River, NJ, 3rd edition, 2002.
13. S. Klose, J. Wang, M. Achtelik, G. Panin, F. Holzapfel, and A. Knoll. Markerless, vision-assisted flight control of a quadrocopter. In *IEEE/RSJ International Conference on Intelligent Robots and Systems (IROS)*, pages 5712–5717, oct. 2010.
14. D. Koditschek. Application of a new Lyapunov function to global adaptive attitude tracking. In *Proceedings of the 27th IEEE Conference on Decision and Control*, pages 63–68, 1988.
15. P. V. Kokotovic, H. K. Khalil, and J. O'Reilly. *Singular Perturbation Methods in Control : Analysis and Design*. Acadademic Press, New York, 1986.
16. D. Lee, H. J. Kim, and S. Sastry. Feedback linearization vs. adaptive sliding mode control for a quadrotor helicopter. *International Journal of Control, Automation, and Systems*, 7:419–428, 2009.
17. T. Lee, M. Leok, and N. H. McClamroch. Geometric tracking control of a quadrotor UAV on SE(3). In *Proceedings of the 49th IEEE Conference on Decision and Control*, pages 5420–5425, 2010.
18. A. Loría and E. Panteley. *Advanced topics in control systems theory : Lecture notes from FAP 2004*, volume 311 of *Lecture Notes in Control and Information Science*, chapter 2 Cascaded Nonlinear Time-Varying Systems: Analysis and Design, pages 23–64. Springer London, 2005.
19. T. Madani and A. Benallegue. Backstepping control for a quadrotor helicopter. In *Proceedings of the IEEE/RSJ International Conference on Intelligent Robots and Systems*, pages 3255–3260, Oct. 2006.
20. F. Mazenc and L. Praly. Adding integrations, saturated controls, and stabilization for feedforward systems. *IEEE Transactions on Automatic Control*, 41(11):1559–1578, 1996.
21. R. Ortega, A. Loría, P. J. Nicklasson, and S.-R. Hebertt. *Passivity-based control of Euler-Lagrange systems: mechanical, electrical and electromechanical applications*. Springer, 1998.
22. E. Panteley and A. Loría. Growth rate conditions for uniform asymptotic stability of cascaded time-varying systems. *Automatica*, 37(3):453–460, Mar. 2001.
23. I. Raptis, K. Valavanis, and W. Moreno. A novel nonlinear backstepping controller design for helicopters using the rotation matrix. *IEEE Transactions on Control Systems Technology*, 19(2):465–473, Mar. 2011.
24. A. Roberts and A. Tayebi. Adaptive position tracking of VTOL UAVs. *IEEE Transactions on Robotics*, 27(1):129 –142, Feb. 2011.
25. P. Seibert and R. Suarez. Global stabilization of nonlinear cascade systems. *Systems & Control Letters*, 14(4):347–352, Apr. 1990.
26. R. Sepulchre, M. Jankovic, and P. Kokotovic. *Constructive Nonlinear Control*. Springer, 1997.
27. E. Sontag. Remarks on stabilization and input-to-state stability. In *Proceedings of the 28th IEEE Conference on Decision and Control*, pages 1376–1378, 1989.
28. E. Sontag. A remark on the converging-input converging-state property. *IEEE Transactions on Automatic Control*, 48(2):313–314, 2003.
29. A. Tayebi and S. McGilvray. Attitude stabilization of a VTOL quadrotor aircraft. *IEEE Transactions on Control Systems Technology*, 14(3):562–571, May 2006.

Dipl.-Ing. Oliver Fritsch
Lehrstuhl für Regelungstechnik,
Technische Universität München, Fakultät Maschinenwesen, Boltzmannstr. 15,
D-85748 Garching bei München,
Fax: +49-(0)89-289-15653
oliver.fritsch@tum.de

Oliver Fritsch arbeitet am Lehrstuhl für Regelungstechnik im Bereich nichtlineare Regelungen. Hauptarbeitsgebiete: Nichtlineare Regelungsstrategien für Quadrocopter.

Dipl.-Ing. David Tromba
Lehrstuhl für Flugsystemdynamik,
Technische Universität München, Fakultät Maschinenwesen, Boltzmannstr. 15,
D-85748 Garching bei München,
Fax: +49-(0)89-289-16058
david.tromba@tum.de

David Tromba hat an der TU München Luft- und Raumfahrt studiert. Arbeitsgebiete in Studienarbeiten am Lehrstuhl für Regelungstechnik: Entwurf und Inbetriebnahme nichtlinearer Quadrocopterregler.

Prof. Dr.-Ing. habil. Boris Lohmann
Lehrstuhl für Regelungstechnik,
Technische Universität München, Fakultät Maschinenwesen, Boltzmannstr. 15,
D-85748 Garching bei München,
Fax: +49-(0)89-289-15653
lohmann@tum.de

Boris Lohmann ist Leiter des Lehrstuhls für Regelungstechnik der Fakultät Maschinenwesen der TU München. Hauptarbeitsgebiete: Modellreduktion, nichtlineare, robuste und optimale Regelung, aktive Schwingungsdämpfung, industrielle Anwendungen.